Asia-Pac. J. Atmos. Sci., 54(1), 19-32, 2018
DOI:10.1007/s13143-017-0053-0
pISSN 1976-7633 / eISSN 1976-7951

Chemical Composition Based Aerosol Optical Properties According to Size Distribution and Mixture Types during Smog and Asian Dust Events in Seoul, Korea

Chang Hoon Jung[1], Ji Yi Lee[2], Junshik Um[3], Seung Soo Lee[4], and Yong Pyo Kim[5]

[1]*Department of Health Management, Kyungin Women's University, Incheon, Korea*
[2]*Department of Environmental Engineering, Chosun University, Gwangju, Korea*
[3]*Department of Atmospheric Sciences, University of Illinois at Urbana-Champaign, Urbana, Illinois, USA*
[4]*Earth System Science Interdisciplinary Center, University of Maryland, College Park, Maryland, USA*
[5]*Department of Chemical Engineering and Materials Science, Ewha Womans University, Seoul, Korea*

(Manuscript received 4 December 2016; accepted 25 April 2017)

Abstract: This study investigated the optical properties of aerosols involved in different meteorological events, including smog and Asian dust days. Carbonaceous components and inorganic species were measured in Seoul, Korea between 25 and 31 March 2012. Based on the measurements, the optical properties of aerosols were calculated by considering composition, size distribution, and mixing state of aerosols. To represent polydisperse size distributions of aerosols, a lognormal size distribution with a wide range of geometric mean diameters and geometric standard deviations was used. For the optical property calculations, the Mie theory was used to compute single-scattering properties of aerosol particles with varying size and composition. Analysis of the sampled data showed that the water-soluble components of organic matter increased on smog days, whereas crustal elements increased on dust days. The water content significantly influenced the optical properties of aerosols during the smog days as a result of high relative humidity and an increase in the water-soluble component. The absorption coefficients depended on the aerosol mixture type and the aerosol size distributions. Therefore, to improve our knowledge on radiative impacts of aerosols, especially the regional impacts of aerosols in East Asia, accurate measurements of aerosols, such as size distribution, composition, and mixture type, under different meteorological conditions are required.

Key words: Aerosol optical properties, smog and Asian dust, aerosol mixture, mass extinction efficiency, water soluble organic carbon

1. Introduction

Aerosol optical properties depend on their physico-chemical characteristics including size distribution, chemical composition, and mixture type. The effect of atmospheric aerosols on the Earth's climate is usually divided into two categories: direct and indirect effects. The direct effect (e.g., Chylek and Coakley, 1974; Schulz et al., 2006) consists of absorption and scattering of radiation by aerosol particles and the indirect effect (e.g., Lohmann and Lesins, 2002; Lohmann and Feichter, 2005) includes the influence of aerosols on cloud radiative properties, as well as on the cloud life cycle. In general, non-absorbing aerosols cause a cooling effect, while absorbing aerosols can produce either cooling or warming effect (e.g., Chylek and Coakley, 1974; Chylek and Wong, 1995).

Aerosols consist of carbonaceous and inorganic species. Carbonaceous species can be classified into organic carbon (OC) and elemental carbon (EC). Organic carbon can be further divided into water soluble organic carbon (WSOC) and water insoluble organic carbon (WISOC) according to their hygroscopic properties. Previous studies have shown that a substantial fraction of OC is water-soluble (Saxena and Hildemann, 1996; Facchini et al., 1999). Thus, it is important to quantify the optical properties of aerosols based on the classified chemical composition including carbonaceous species along with the relation with relative humidity and water content.

Other important properties for understanding aerosols effects are their polydispersity and mixing state. Atmospheric aerosols that are distributed over a broad range of sizes are considered to be polydisperse. For example, aerosol optical properties depend strongly on their size distribution parameters, such as a geometric mean diameter (d_g) and geometric standard deviation (σ_g) (Seinfeld and Pandis, 1998; Jung et al., 2015). Assumptions regarding aerosol mixing state also cause uncertainties in modeling of aerosol optical properties. Some models consider aerosols to be internally mixed, whereas others assume an external mixture (e.g., Textor et al., 2006). Therefore, to quantify the contributions of each composition to the total optical properties of aerosol, it is important to understand the characteristics of each aerosol, including their size distributions and mixture types, as well as chemical composition.

In this study, aerosol optical properties were investigated for different meteorological events including smog and Asian dust events in Seoul, a representative urban site of Korea. The acquired data from the smog and Asian dust events were compared with those obtained from normal days during the sampling period. The measurements were then used to perform a sensitivity test using size distributions with varying geometric mean diameters and geometric standard deviations. These size- and composition-resolved aerosol optical properties were cal-

Corresponding Author: Chang Hoon Jung, Department of Health Management, Kyungin Women's University, 63, Gyeyangsan-ro, Gyeyang-gu, Incheon 21041, Korea.
E-mail: jch@kiwu.ac.kr

culated based on the Mie theory. The influence of the aerosol mixing states on the optical properties was also determined assuming fully external, internal and EC/non-EC aerosol mixtures. The detailed description of the aerosol mixtures was explained in the Appendix.

2. Measurements

In this study, PM2.5 samples were collected in Seoul between 25 and 31 March, 2012 using a high-volume sampler (1000 L min^{-1}). The sampling site was at the Korea Institute of Science and Technology (KIST), which is located within a residential area in the northeast of Seoul (Fig. 1). The sampling point was on the roof of a two-story building (58 m above sea level) at KIST, approximately 7 km from the center of Seoul. Organic carbon and elemental carbon in the sample filters were analyzed using a Sunset OC/EC analyzer (Sunset Laboratory, Tigard, Oregon, USA) based on a thermal/optical transmittance method. The sample filter was first heated in helium in four temperature steps: 300°C, 450°C, 600°C, and 870°C, to volatilize OC. Temperature was briefly reduced before the carrier gas was switched to 1% oxygen in helium, followed by multiple temperature increases up to 870°C to combust EC and pyrolyzed carbon. Pyrolytically generated EC from charring of OC was corrected using filter transmittance (Birch and Cary, 1996).

A portion (3 cm × 5 cm) of the 203 mm × 254 mm quartz filter was extracted by ultra-sonification using 40 mL deionized water twice for 30 min to quantify WSOC. Ice water was used in the sonication bath to minimize possible loss of volatile OC due to temperature increase during extraction. Filter debris and suspended insoluble particles were removed from the extracts using a syringe filter (0.2-μm PTFE membrane, PALL science, New York, USA). WSOC analyses were performed using a TOC-V_{CPH} organic carbon analyzer (Shimadzu corporation, Kyoto, Japan). In this study, the mass concentrations of organic matter (OM) and water soluble organic matter (WSOM) were estimated by multiplying the OC and WSOC concentrations by 1.6 (OM = OC × 1.6) and 2.1 (WSOM = WSOC × 2.1),

Fig. 1. Location of the sampling site (KIST, Seoul, Korea). The map in the figure shows the northeast part of Asia and the red circle marks the Seoul area. In the Seoul area, red asterisk marks the sampling site.

Table 1. Meteorological condition, relative humidity, and classified event for each sampling day (top portion). Measured concentration of each PM2.5 composition for each sampling day (bottom portion).

Sampling date		25 March	26 March	27 March	28 March	30 March	31 March
Meteorological condition		Sunny, Windy	Sunny, Windy	Cloudy	Cloudy	After rain, Cloudy	Heavy Cloudy, Windy
Relative humidity (%)		36.6	38.3	57.6	56.4	73.5	38.4
Classified event		Normal	Normal	Smog	Smog	Smog	Asian Dust
Chemical composition in PM2.5 (Unit: μg m^{-3})							
Carbonaceous	EC	1.43	1.71	2.20	2.14	1.88	2.14
	OM	8.11	11.16	10.28	19.73	10.73	13.21
Water soluble/insoluble organic matter	Soluble (WSOM)	5.91	7.71	10.01	14.88	10.70	7.50
	Insoluble (WISOM)	2.20	3.45	0.27	4.85	0.03	5.71
Anion	Cl^-	0.24	0.45	0.36	0.45	0.35	1.42
	NO_3^-	1.51	4.70	12.22	10.93	6.08	2.32
	SO_4^{2-}	4.03	3.95	11.42	18.23	10.71	6.66
Cation	Ca^{2+}	0.26	0.26	0.27	0.34	0.44	1.53
	Mg^{2+}	0.11	0.06	0.08	0.07	0.31	0.44
	K^+	0.36	0.41	0.54	0.71	0.48	3.20
	Na^+	0.42	0.54	0.68	0.58	0.45	4.67
	NH_4^+	1.72	2.71	6.33	6.71	4.44	3.75
Total		18.20	25.94	44.37	59.90	35.87	39.33

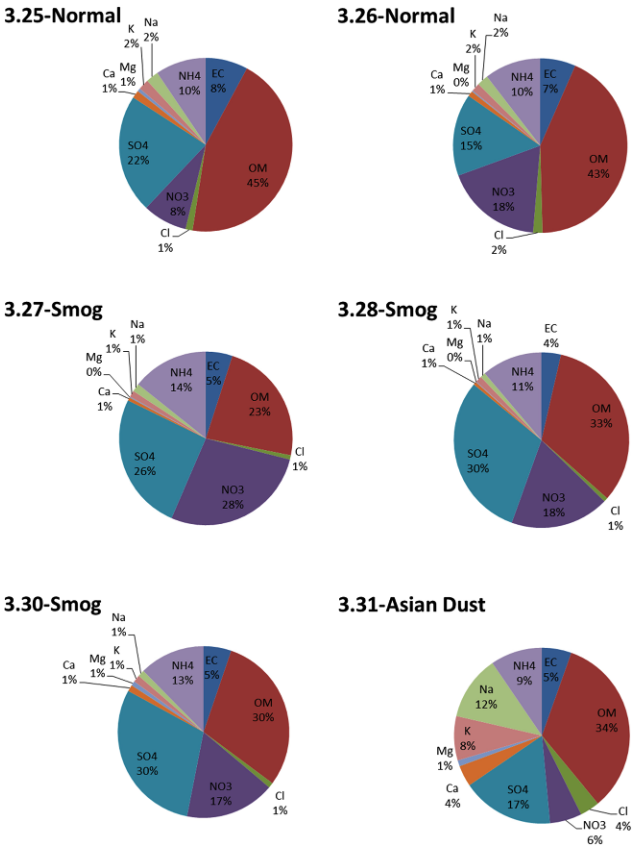

Fig. 2. Measured chemical compositions in PM2.5 on each day during the sampling period: 25 March (top left), 26 March (top right), 27 March (middle left), 28 March (middle right), 30 March (bottom left), and 31 March (bottom right).

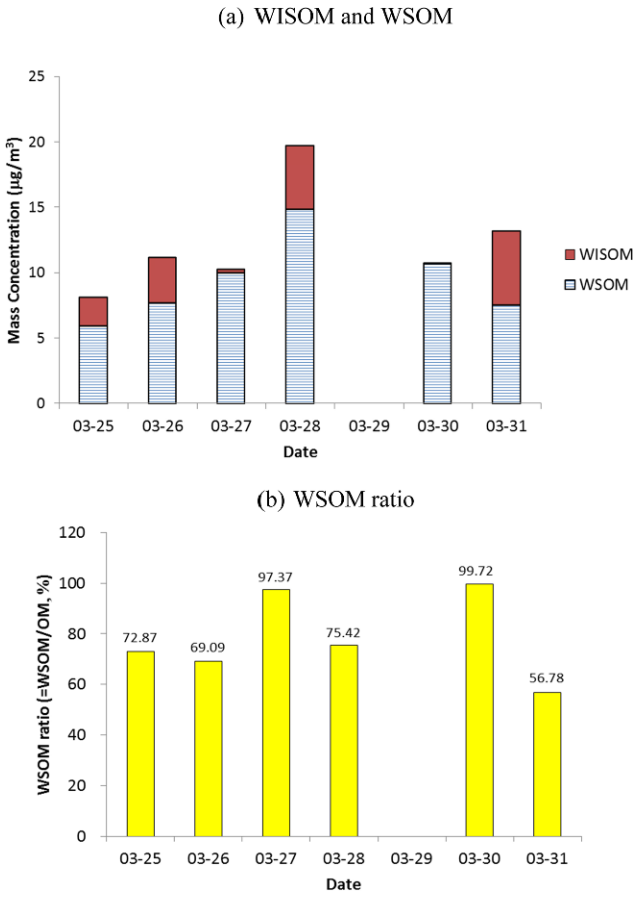

Fig. 3. (a) Relative contribution of water soluble organic matter (WSOM) and water insoluble organic matter (WISOM) and (b) the ratio of WSOM to all organic matter (OM), during the sampling period (OM = 1.6 × OC; WSOM = 2.1 × WSOC). In panel (b), numbers above the yellow boxes are the ratio in percent on each day.

respectively (Turpin and Lim, 2001). The water insoluble organic matter (WISOM) concentration was calculated by subtracting the WSOM concentration from the OM concentration.

Ion components, SO_4^{2-}, NO_3^-, Cl^-, NH_4^+, K^+, Ca^{2+}, Na^+, and Mg^{2+}, were analyzed by extracting water-soluble species in a shaker using 20 mL of distilled and deionized water for 120 min. Anions were analyzed using an ion chromatography (2000i/sp, Dionex, CA, USA). Cations, except for NH_4^+, were analyzed using an atomic absorption spectroscopy, whereas NH_4^+ was analyzed by an indophenol colorimetric method using a spectrophotometer (Genesys2, Spectronic Instrument, New York, USA). The limits of detection were less than 0.01 μg m^{-3} for the anions and 0.006 μg m^{-3} for the cations. The mass concentration and contribution of EC, OM, and inorganic ions (NH_4^+, SO_4^{2-}, and NO_3^-, hereafter called AMS) within PM2.5 are given in Table 1.

We classified event days and normal days based on the PM2.5 mass concentration. When the daily average PM2.5 mass concentration was over 100 μg m^{-3}, which was two times higher than the 24-hr National Air Quality Standard value (50 μg m^{-3}) for PM2.5 in Korea, we classified these days as event days. We further differentiated these event days into smog day and Asian dust day. On 31 March, Korea Meteorological Administration announced an Asian dust event in Incheon and Gyeonggi province that encompasses Seoul. High PM10 mass concentrations were reported at metropolitan urban air quality monitoring stations on that day. For example, several stations at Incheon (2 stations at Namdong-Gu) and Gyeonggi province (8 stations including Gimpo, Goyang, and Bucheon) reported that PM10 concentration was over 300 μg m^{-3} in the afternoon (0600-0900 UTC). For these reasons, we also designated this day as an Asian dust day in the Seoul metropolitan area.

Figure 2 shows daily PM2.5 compositions during the sampling period. For normal days, OM was the most abundant aerosol and contributes up to 45% (25 March) and 43% (26 March) of PM2.5. The contribution of EC was minor: minimum of 4% on 28 March and maximum of 8% on 25 March. During smog days (27, 28, and 30 March), the contribution of sulfate increased up to 30% (28 March) from 15% on normal day (26 March), while the contribution of OM decreased to 23% (27 March) from 45% (25 March). The concentrations of NH_4^+ and of mineral compounds, such as

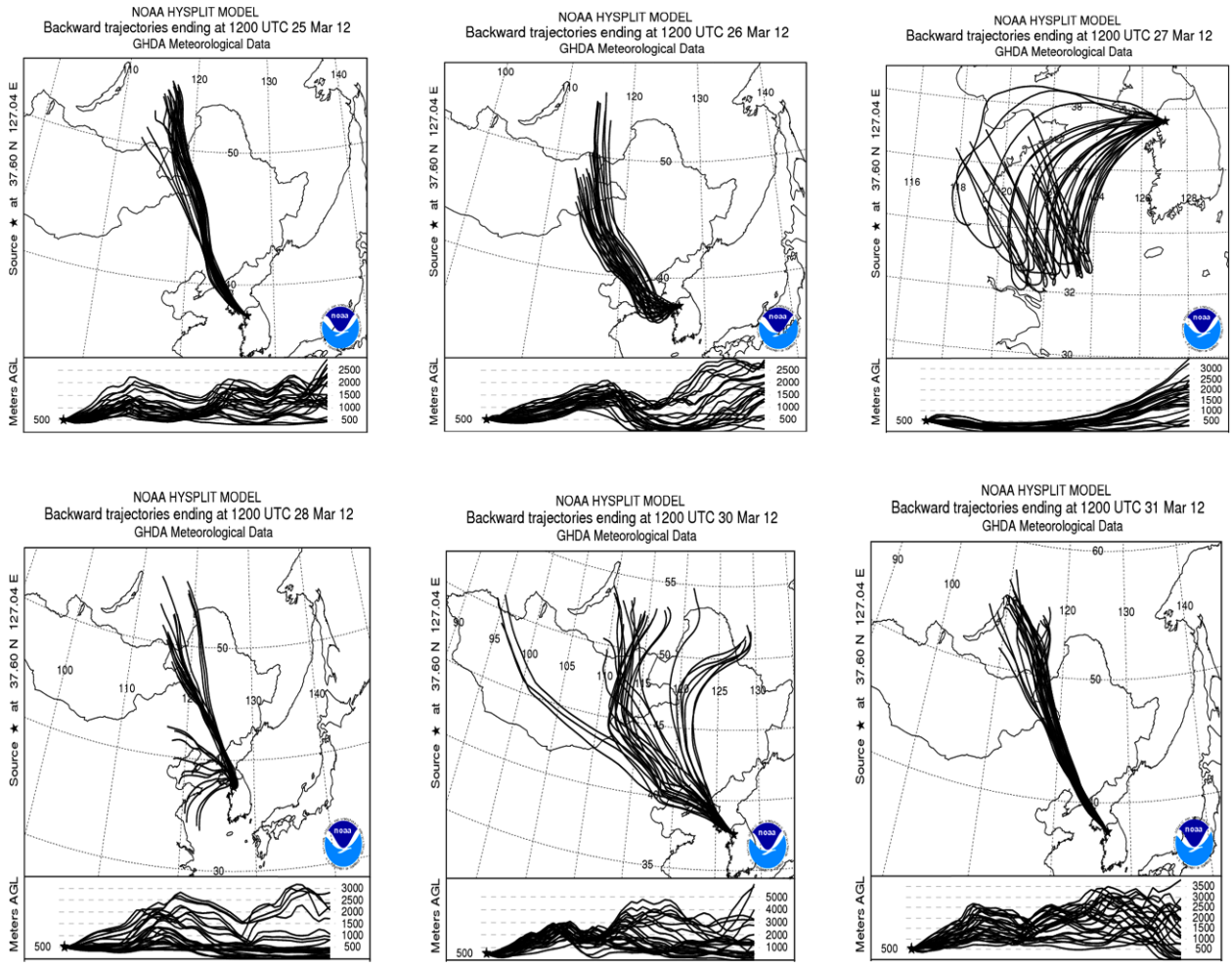

Fig. 4. 2-day backward trajectories traced by the NOAA Hybrid Single Particle Lagrangian Integrated Trajectory (HYSPLIT) model with endpoints in KIST for 1200 UTC. The trajectory ensemble shows multiple trajectories from the selected starting location and suggests 27 members for all possible offsets. Each black line represents an air mass trajectory. The upper part of each panel shows the projected paths of the trajectories on the surface, while the bottom panel shows the vertical variations of trajectories over the projected paths. One end of each black line in Korea and on the left hand side in the bottom panels mark the endpoint of each trajectory in KIST, while the other end of each line marks the starting point.

Na^+, Ca^{2+}, Mg^{2+}, and K^+, did not show significant difference between smog and normal days. However, the contribution of mineral compounds increased during dust event, and this is mainly due to the dust composition. The AMS (NH_4^+, SO_4^{2-}, and NO_3^-) and PM2.5 mass concentrations in the smog days were two times higher than those in normal days, whereas the average mass ratio of AMS in PM2.5 during the smog days was approximately 46%. However, the mass ratio of AMS in PM2.5 decreased to 32% during the Asian dust day.

Although there were large variations in aerosol concentrations, measurement procedures, and sampling periods, several studies showed the common characteristics of aerosol chemical composition during Asian dust and smog days (e.g., Huang et al., 2014; Boreddy and Kawamura, 2015). For example, the mass concentration of mineral ions, such as Na^+, Ca^{2+}, and Cl^-, which came mainly from natural dust sources, was higher during Asian dust days compared to normal or smog days. For smog days, the general aerosol characteristics showed that major aerosol chemical species, such as SO_4^{2-}, NO_3^-, NH_4^+, and Cl^-, were positively correlated with relative humidity. For instance, Huang et al. (2014) showed that SO_4^{2-} increased approximately 5 fold, while NO_3^- and NH_4^+ increased approximately 3 fold during smog days in Beijing. This study also shows the same general chemical composition characteristics that have been reported in previous studies during smog and Asian dust days.

Figure 3 shows that the contribution of WSOM was dominant during smog days. The mass ratio of WSOM to OM was 69-73% during normal days. However, the WSOM mass ratio increased during smog days, especially on 27 and 30 March, which indicates a different origin of OM compared with normal days, at least during those specific smog days.

During the Asian dust day, the mass ratio of WSOM to OM decreased to 57%.

Figure 4 shows the 2-day backward trajectories of air masses traced by the NOAA Hybrid Single Particle Lagrangian Integrated Trajectory (HYSPLIT) model with endpoints at KIST, Seoul for 1200 UTC. HYSPLIT is a complete system for computing simple air parcel trajectories as well as complex transport, dispersion, chemical transformation, and deposition simulations (Draxler and Hess, 1998).

Figure 4 shows that air masses came mostly from the northeast continental Asia during the sampling period. However, air masses moved from the eastern coast of China to Seoul through the west coast of Korea on 27 March. Thus, these air masses were likely to include and transport aerosols that originated from those coastal areas and affected the measurements on smog day of 27 March. For the case of 28 March, air masses originated from both the northeast continental Asia and the east coast of China. This indicated that the smog day of 28 March was likely to be affected by aerosols transported from both continental and coastal areas. In order to further specify the origin of the air mass, more detailed studies are required. As Fig. 4 shows, most backward trajectories appear to be from China. Thus, it is difficult to differentiate the absolute origin of smog from the domestic origin due to long range transportation.

3. Model description

In this study, the aerosol optical properties were calculated by considering hygroscopicity, size distribution, and mixing state of aerosol particles. Figure 5 shows a schematic diagram for the model procedure. We assume that aerosols are composed of AMS, EC, OM, NaCl, crustal (K^+, Mg^{2+}, Ca^{2+}), and water compositions.

Composition-based aerosol optical properties are closely related to a wavelength (λ) of incident light and refractive index and size distribution of aerosols. Table 2 shows the refractive indices and densities of aerosol compounds at λ = 550 nm (Hess et al., 1998, Lesins et al., 2002). Based on the given conditions, the optical properties of aerosols were calculated using the Mie theory. Internal, fully external, and EC/non-EC mixtures were used for these calculations. The water contents at a given relative humidity and chemical composition were calculated using an aerosol thermodynamics model (SCAPE II, Kim et al., 1993). A more detailed description of the model development is explained in the Appendix.

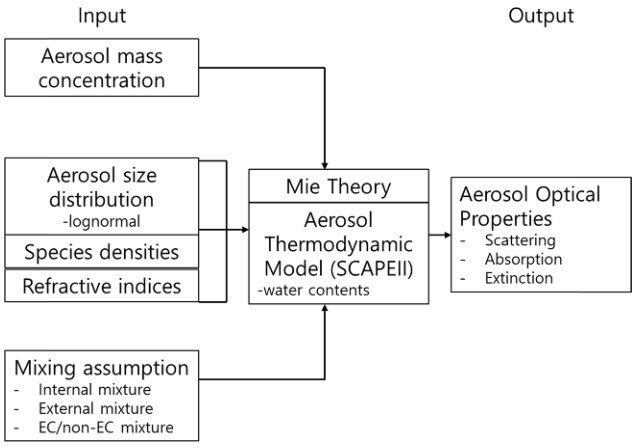

Fig. 5. Schematic diagram that depicts how aerosol optical properties are calculated in the model.

Table 2. Refractive indices and densities of the various aerosol components (Hess et al., 1998; Lesins et al., 2002) at λ = 550 nm.

	Refractive index	Density (g cm^{-3})
EC	$1.75\text{-}4.4 \times 10^{-1}$i	1.0
Inorganic ions (AMS)	1.43	1.7
OM	$1.53\text{-}6.0 \times 10^{-3}$i	1.2
NaCl	$1.5\text{-}1.0 \times 10^{-8}$i	2.2
Crustal	$1.53\text{-}1.1 \times 10^{-3}$i	2.6
Water	1.33	1.0

Many studies have used mass concentration to calculate the optical properties of aerosols without corresponding size distribution. However, aerosol size distributions play an important role in characterizing the optical properties. In this study, we quantified the sensitivity of the calculated optical properties to the assumed aerosol size distributions.

4. Results and discussion

a. Optical properties of different mixtures during the sampling period

Figure 6 shows the variations in composition-based mass concentration including water contents calculated using a thermodynamic model (SCAPE II, Kim et al., 1993), extinction coefficient, and absorption coefficient during the sample period. A lognormal size distribution was assumed and a geometric mean diameter (d_g) of 0.2 μm and a geometric standard deviation (σ_g) of 1.5 were used as representative values for these calculations. When using a lognormal size distribution to represent polydisperse size distribution of aerosols, nuclei mode aerosols have been generally assumed to have geometric mean diameters of 0.1-1.0 μm with various geometric standard deviations. For this study, we selected a geometric mean diameter of 0.2 μm because it was the representative geometric mean diameter of fine mode aerosols used in previous studies (e.g., John et al., 1990; Hovart et al., 1996; Kim et al., 2007) with a geometric standard deviation of 1.5 (e.g., Chung et al., 2012; Liu et al., 2016). It is noted that these values should vary with meteorological and measurement conditions. In this study, we calculated the optical properties using a wide range of geometric mean diameters (0.1-1.0 μm) and geometric standard deviations (1.3-2.2).

The water contents calculated using the thermodynamic

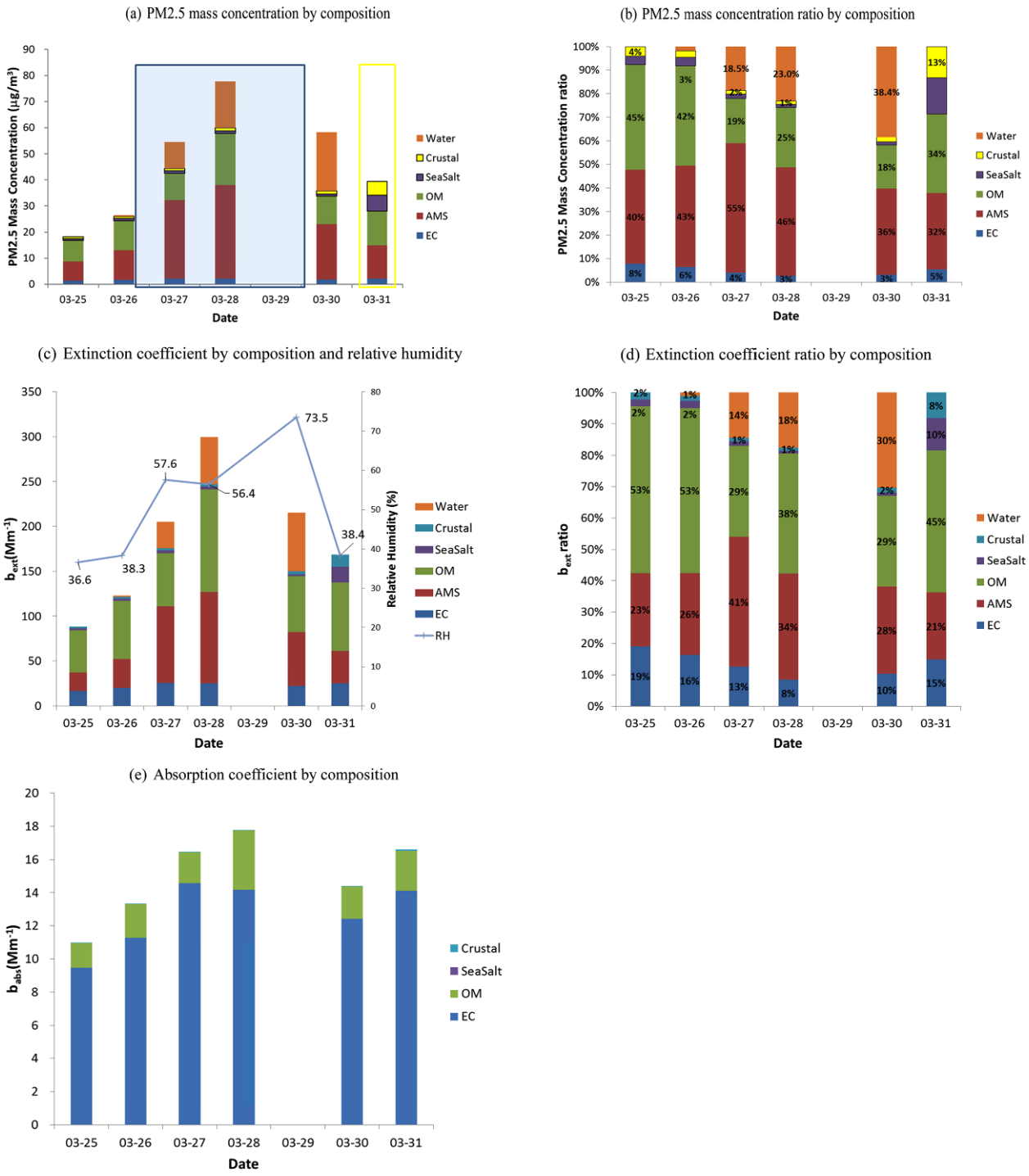

Fig. 6. Aerosol composition-based (a) mass concentration [blue rectangle: the period with smog (27, 28, and 29 March), yellow rectangle: the period with Asian dust (31 March)], (b) mass concentration ratio in PM 2.5, (c) extinction coefficient with relative humidity (blue line), (d) extinction coefficient ratio, and (e) absorption coefficient with fully external aerosol mixture types (d_g = 0.2 μm, σ_g = 1.5, PM2.5) at λ = 550 nm, taken from the model simulation results.

model (SCAPE II) were between 0 μg m^{-3} (0%) and 0.46 μg m^{-3} (1.74%) for 25 and 26 March, respectively, as shown in Fig. 6a (Fig. 6b), and the corresponding relative humidity (RH) were 36.6% and 38.3% (Fig. 6c). For smog days, the RH increased to 73.5% (30 March) from 56.4% (28 March) and the water contents increased to 22.33 μg m^{-3} (30 March) from 17.9 μg m^{-3} (28 March), which affected the optical properties as shown in Figs. 6c and 6d. Figure 6e shows that the main

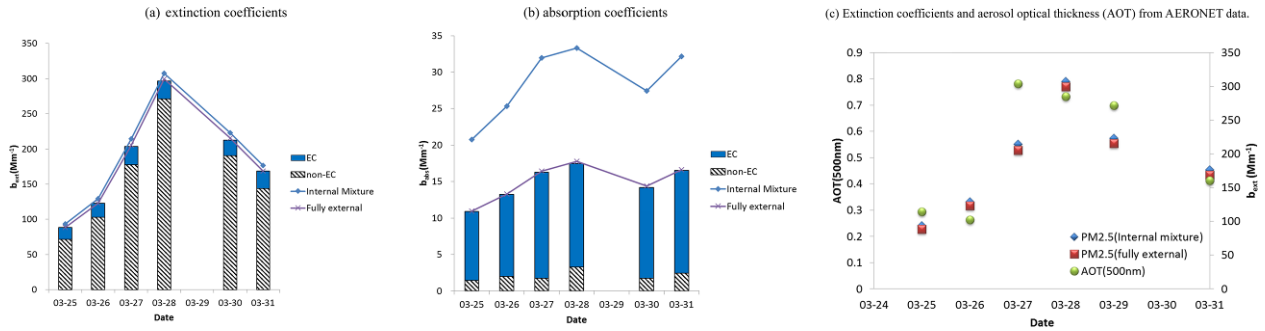

Fig. 7. The calculated (a) extinction coefficients, (b) absorption coefficients for different aerosol mixture types (i.e., internal mixture and fully external mixture), and (c) a comparison between the calculated extinction coefficients of different mixture types in this study and the determined aerosol optical thickness (AOT) from AERONET data.

contributors to the extinction coefficient were EC and OM. The average OM (EC) contribution to the total absorption coefficient was 17.37% (82.63%). The maximum contribution of OM was 25.28% on 28 March, while it was 87.18% on 27 March as shown in Fig. 6e.

Figure 7a shows a comparison of the calculated extinction coefficients with different aerosol mixture types during the sample period. A lognormal size distribution with $d_g = 0.2$ μm and $\sigma_g = 1.5$ were assumed for this calculation. The internal, EC/non-EC, and fully external mixture were compared. The extinction coefficients for different mixtures showed comparable results in terms of their values and trends. The internal mixture showed slightly higher extinction coefficients than those of fully external and EC/non-EC mixtures. On average, the extinction coefficients calculated assuming an internal mixture were 4.23% higher than those with fully external mixtures. Figure 7b shows the calculated absorption coefficients during the sampling period. The absorption coefficients of EC with an internal mixture were 91% higher than those of fully external and EC/non-EC mixtures, on average. For the internal mixture, the refractive index was calculated as an average volume of each composition, which resulted in the corresponding simulation differing from that of the external mixture.

In addition to the calculations of extinction and absorption coefficients shown in Figs. 7a and 7b, a comparison between the extinction efficient and the determined aerosol optical thickness (AOT) from the Aerosol Robotic Network (AERONET) remote sensing data was made. The purpose of this comparison is to investigate how the component resolved aerosol optical properties can be related to the total aerosol optical properties based on the measurement. The determined AOT from AERONET data does not provide information of aerosol composition. However, the optical properties calculated from this study can indicate the influence of chemical composition on the aerosol optical properties, such as the contribution of each chemical composition to the total aerosol optical properties. Figure 7c shows a comparison between the calculated aerosol extinction coefficients in this study and the AERONET AOT (at Seoul National University, Seoul) during

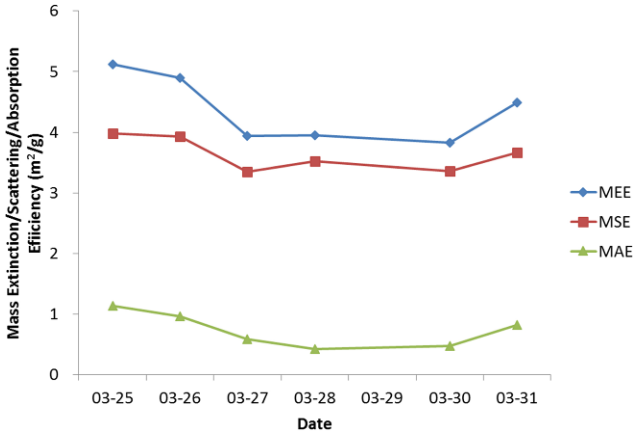

Fig. 8. The mass extinction (MEE), scattering (MSE), and absorption efficiency (MAE) of PM2.5 during the sampling period. Internal mixture, $d_g = 0.2$ μm, and $\sigma_g = 1.5$ were assumed for aerosols at $\lambda = 550$ nm.

the sampling period. Both internal and fully external mixtures were considered. As Fig. 7c shows, the AOT and extinction coefficients for the internal and fully external mixtures are correlated well each other. It is difficult to directly compare the calculated optical properties using different processes and assumptions, i.e., the calculated optical properties of aerosols based on chemical composition and remotely observed AERONET data, because of several limitations. It should be noted that the sampled PM2.5 measurements may have missing particles in the coarse mode. A comparison of the ground based measurements with columnar observations clearly shows different behaviors. Sun photometer data (i.e., AERONET) were obtained during daytime and cloud free conditions, which might cause differences from the 24-hr sampled data. However, the purpose of this comparison is to test whether the technique developed in this study (i.e., calculation of aerosol optical properties based on chemical compositions) can also capture the trend shown in aerosol optical properties acquired by independent observations.

Figure 8 shows the changes in mass extinction (MEE), scattering (MSE), and absorption efficiency (MAE) of PM2.5

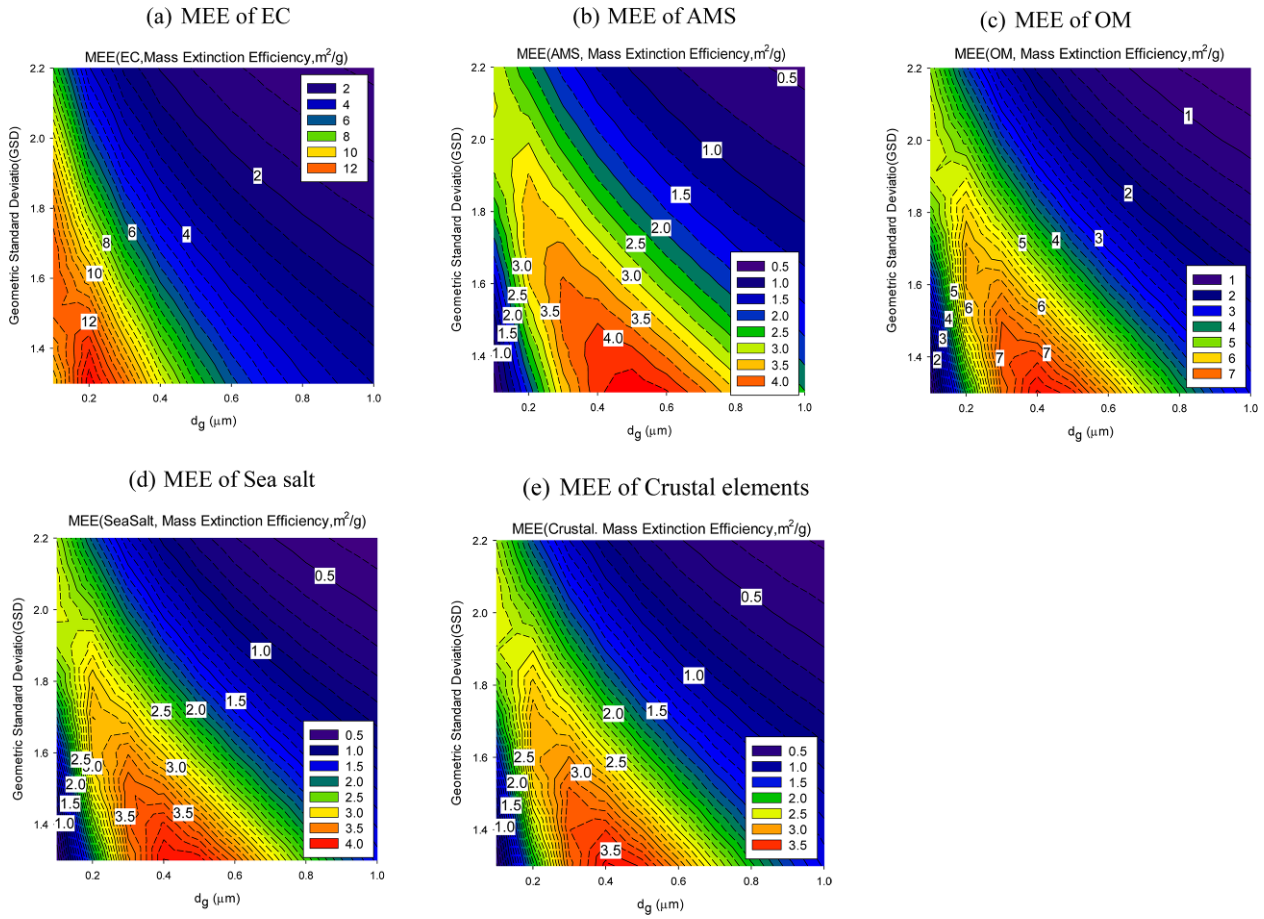

Fig. 9. Mass extinction efficiency (MEE) as a function of the geometric mean diameter (d_g) and geometric standard deviation (GSD) for each aerosol component at $\lambda = 550$ nm.

during the sampling period. An internal mixture, $d_g = 0.2$ μm, and $\sigma_g = 1.5$ were assumed for this calculation at $\lambda = 550$ nm. It was shown that the MEE, MSE, and MAE decreased during the smog days compared with normal and Asian dust days. For example, the MEE, MSE, and MAE were 3.83 $m^2\ g^{-1}$, 3.36 $m^2\ g^{-1}$, and 0.47 $m^2\ g^{-1}$, respectively, on 30 March, which were lower than those on normal days (MEE, MSE, and MAE of 5.12 $m^2\ g^{-1}$, 3.98 $m^2\ g^{-1}$, and 1.14 $m^2\ g^{-1}$, respectively, on 25 March). The main reason for such decreases during smog days can be explained by the increase in water content, which reduced scattering and absorption in the internally mixed aerosols and hence decreased the mass scattering and absorption efficiencies. During smog days, the water content increased because of relative humidity and thermodynamic characteristics of aerosol composition (e.g., Kim et al., 1993). Higher relative humidity indicates a greater amount of moisture in the air for a given temperature. For an air parcel with higher relative humidity, moisture readily condenses onto the pollution particles. Thus, an extinction coefficient is larger during smog days because of the high relative humidity. Because the mass efficiencies (i.e., MEE, MSE, and MAE) are defined as the ratio of the extinction coefficient to mass concentration, the MEE and MSE can show different trends compared with b_{ext} or b_{sca}. For smog days, b_{ext} and the mass concentration of water were much higher than other days. However, the increase in water mass concentration on smog days was larger than the increase in the b_{ext} of water, which caused the decrease in MEE and MSE. During Asian dust day, water contents did not have an influence on the optical properties due to low RH. However, the increase in crustal elements reduced the mass scattering efficiencies compared with those of normal days, although this influence was not significant.

It should be noted that the results shown in Figs. 6-8 are based on a fixed size distribution with a geometric standard deviation of 1.5 and a geometric mean diameter of 0.2 μm. The actual optical properties of aerosols depend heavily on the assumed size distributions, even for the same mass concentration of aerosols. For this reason, the sensitivity of aerosol optical properties to assumed size distributions should be investigated. A detailed sensitivity study for aerosol size distribution is considered in the following section.

Table 3. Maximum and minimum of MEE, MSE, and MAE of each aerosol component for the range of geometric mean diameter (d_g) between 0.1 and 1.0 μm and that of geometric standard deviation (σ_g) between 1.3 and 2.2.

	MEE		MSE		MAE	
	Min.	Max.	Min.	Max.	Min.	Max.
OM	0.620	7.939	0.502	7.629	0.109	0.223
EC	0.728	13.481	0.3897	5.534	0.3384	8.121
Inorganic ions (AMS)	0.388	4.461	0.388	4.461	-	-
Sea Salt	0.339	4.006	0.339	4.006	-	-
Crustal	0.286	3.636	0.272	3.618	0.009-	0.021

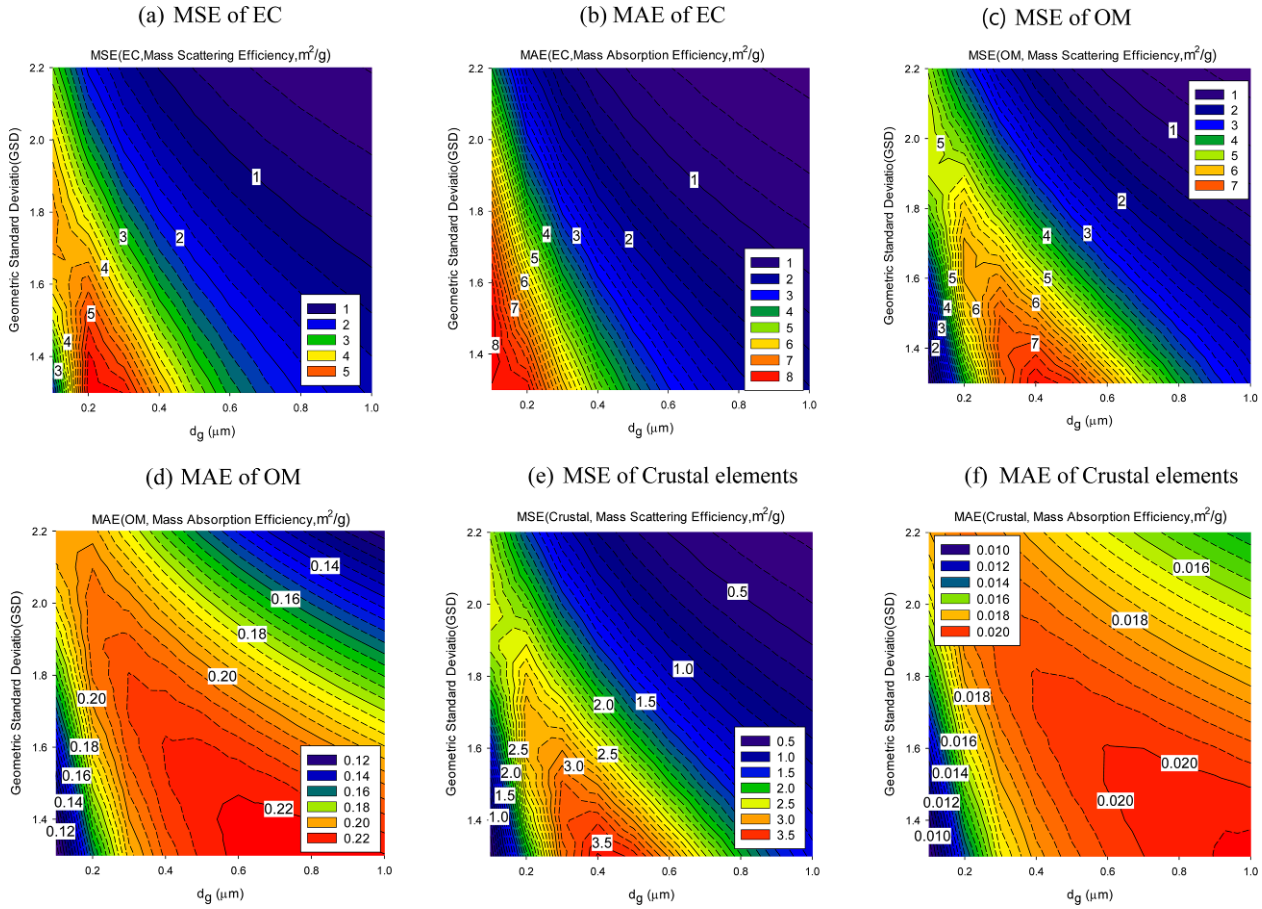

Fig. 10. The MSE (left column) and MAE (right column) of EC (top panels), OM (middle panels), and crustal elements (bottom panels) at λ = 550 nm.

b. Sensitivity tests of optical properties to size distribution parameters

In this study, we assumed lognormal size distributions to represent the polydispersity of aerosol particles. Figure 9 shows the sensitivity of the MEE as functions of geometric mean diameter and geometric standard deviation for each composition. It shows that the MEE varies significantly with different size distributions (i.e., different d_g and σ_g). Table 3 summarizes the calculated ranges of MEE, MSE, and MAE for each composition within the given simulation conditions of the geometric mean diameter (d_g) and geometric standard deviation (σ_g). For example, the MEE of EC varies from 0.728-13.481 $m^2\ g^{-1}$ for geometric mean diameters of 0.1-1.0 μm and geometric standard deviations of 1.3-2.2. In general, the MEE decreases with increasing geometric mean diameter and geometric standard deviation. This implies that small particles with a narrow distribution (i.e., small geometric standard

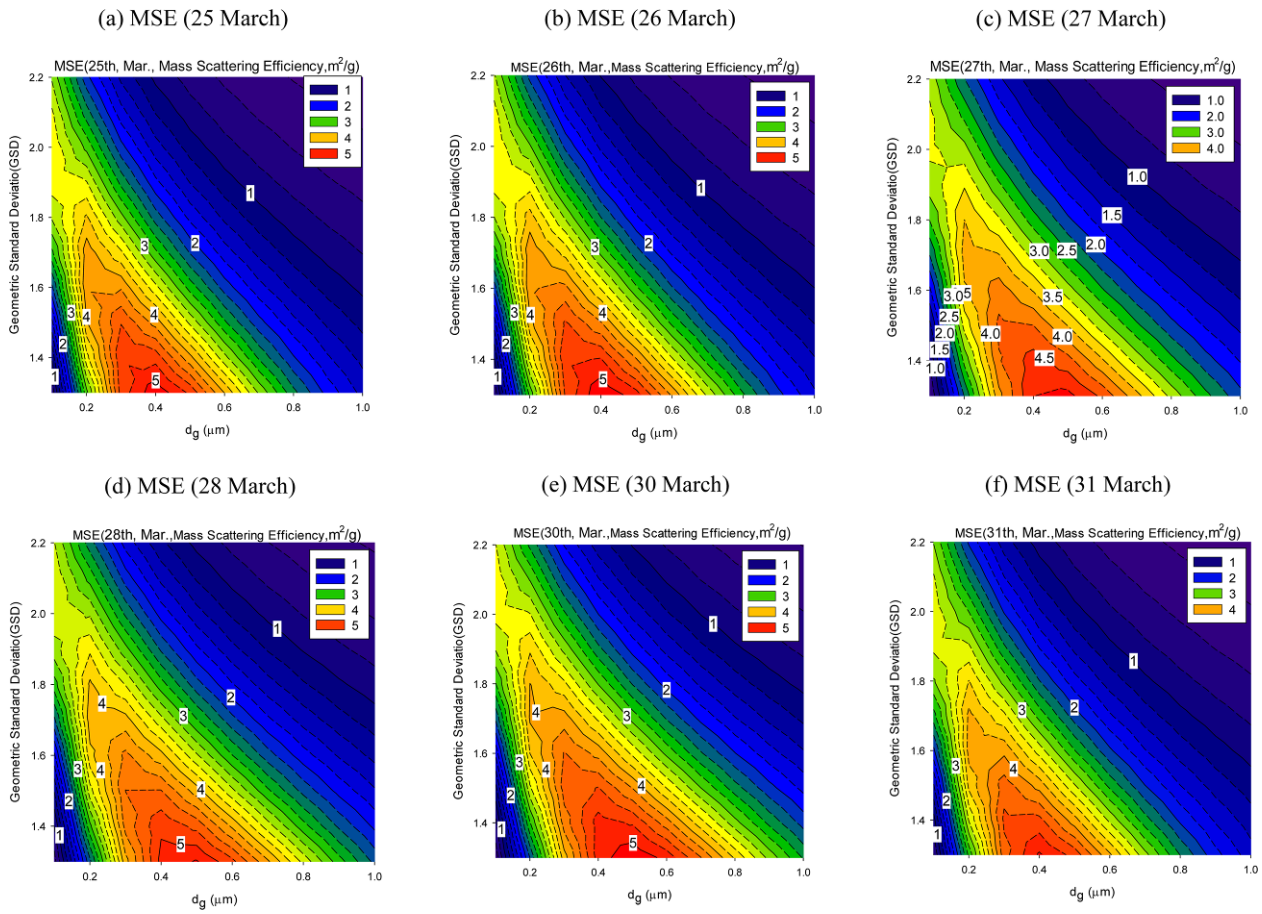

Fig. 11. Calculated MSE for polydisperse aerosols during the sampling period at $\lambda = 550$ nm. Each panel represents a different sampling day.

deviation) have a higher MEE than larger particles with a wide size distribution. This trend is also shown for other compositions with the geometric mean diameters larger than 0.3 μm, yet trends vary with composition. Figure 9 also shows that the MEE of the EC and OM are larger than those of other compositions, which indicates that the contributions of OM and EC, such as crustal and inorganic ions, are also larger.

Figure 10 shows the calculated MSE and MAE of EC, OM, and crustal elements. By comparing Figs. 9 and 10, it is clear that the MSE and MEE of OM and crustal elements are comparable (i.e., minimum absorption). The MAE from the absorbing aerosol is mostly due to EC, although the detailed contribution of optical properties depends on their mass concentration. Figures 11 and 12 show the sensitivity of MSE and MAE for polydispersed aerosols during the sampling period. The MSE and MAE decrease with an increase in the geometric mean diameter and a decrease in the geometric standard deviation, when the geometric mean diameter is larger than approximately 0.4 μm. However, there is an increasing trend for both MSE and MAE, for smaller particles (< ~0.4 μm in diameter), as the geometric mean diameter increases. Figures 11 and 12 also show that a maximum mass extinction efficiency exists for a given size distribution. Table 4 shows the ranges of calculated MEE, MSE, and MAE during the sampling period with the assumed geometric mean diameters (d_g) and geometric standard deviations (σ_g) of 0.1-1 μm and 1.3-2.2, respectively. Subsequently, Figs. 9-12 show how the size distribution can significantly influence the aerosol optical properties.

c. Optical properties of WSOM

Large uncertainties in the optical properties of OM are mainly due to the variety of WSOM. One of the most uncertain characteristics of WSOM is their light absorption properties. The light absorption properties of WSOM are commonly represented using an imaginary part of the aerosol refractive index. Because individual WSOM has a wide range of imaginary part of refractive index, we only simulated the optical properties of WSOM for the sensitivity test. In this study, we used 0.01 to 0.3 to represent the imaginary part of the refractive index of WSOM. Figure 13 shows the maximum, minimum, and mean of the calculated extinction and absorption coefficients of WSOM during the sampling period.

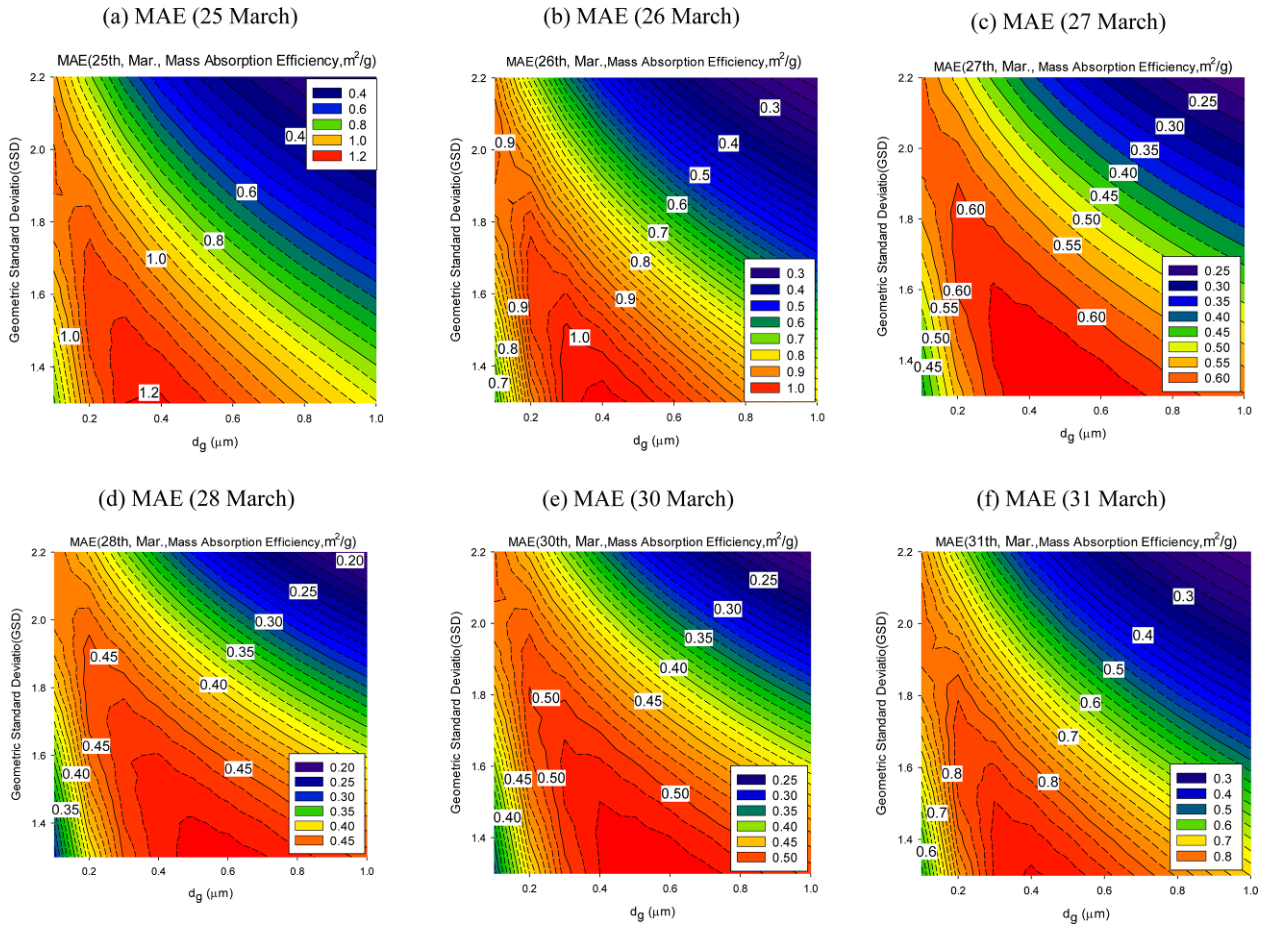

Fig. 12. Calculated MAE for polydisperse aerosols during the sampling period at $\lambda = 550$ nm. Each panel represents a different sampling day.

Table 4. Maximum and minimum of MEE, MSE, and MAE on each day during the sampling period for the range of geometric mean diameter (d_g) between 0.1 and 1.0 μm and that of geometric standard deviation (σ_g) between 1.3 and 2.2.

Internal mixture	MEE		MSE		MAE		Classified event
	Min.	Max.	Min.	Max.	Min.	Max.	
25 March	0.531	6.353	0.296	5.145	0.235	1.208	Normal
26 March	0.530	6.221	0.303	5.190	0.227	1.031	
27 March	0.538	5.476	0.335	4.823	0.204	0.647	Smog
28 March	0.562	5.703	0.376	5.219	0.186	0.485	
30 March	0.598	5.695	0.396	5.167	0.202	0.528	
31 March	0.479	5.713	0.277	4.829	0.202	0.884	Asian Dust

In Fig. 13, the imaginary part of the refractive index of WSOM ranges from 0.01 to 0.3, assuming a fixed aerosol size distribution with $d_g = 0.2$ μm and $\sigma_g = 1.5$ at $\lambda = 550$ nm. The extinction coefficients during normal days and smog days have values of 31.27-51.37 Mm^{-1} and 52.96-99.14 Mm^{-1}, respectively, and smog days have larger variations in extinction coefficients than normal days. The absorption coefficients have values between 1.54 and 29.48 Mm^{-1} for normal days and 2.61-56.90 Mm^{-1} for smog days. Subsequently, the sensitivity test shows that the calculated absorption coefficients have wider ranges than the extinction coefficients. Smog days show higher coefficient values compared with normal days.

5. Concluding remarks

Aerosol optical properties were investigated using data

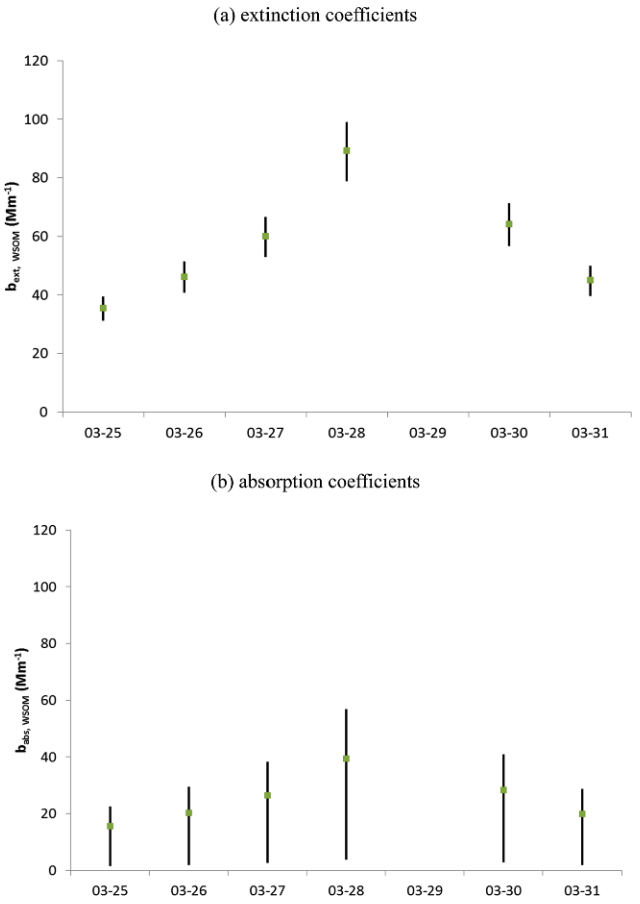

Fig. 13. The range of (a) extinction coefficients and (b) absorption coefficients of WSOM during the sampling period. The squares are mean values and the minimum and maximum values are added vertically. The imaginary part of the refractive index of WSOM between 0.01 and 0.3 and d_g=0.2 μm and σ_g = 1.5 were used at λ = 550 nm.

acquired in Seoul (25-31 March, 2012), which is a representative urban site in Korea. Different meteorological events, such as smog and Asian dust event, were observed during the sampling period. PM2.5 was measured, along with compositions of water soluble organic matter (WSOM), water insoluble organic matter (WISOM), and elemental carbon (EC), as well as inorganic species. The analyzed measurements showed that the concentration of inorganic ions (AMS including NH_4^+, SO_4^{2-}, and NO_3^-) increased during smog days, while sea-salt and crustal aerosol ions, such as Na^+, Ca^{2+}, and K^+, increased during dust days. Among organic matter (OM), the contribution of WSOM increased to 99.72% during smog days and decreased to 57% during Asian dust day. This indicated that the origin of OM differed from normal days and depended on meteorological conditions.

This study quantified the effects of aerosol composition and mixture types on the optical properties of aerosols calculated using the acquired measurements and the Mie theory. The influence of the aerosol mixture on optical properties was determined using assumptions of internal, EC/non-EC, and fully external aerosol mixtures. It was found that the calculated extinction coefficient for internal mixtures was 4.23% larger than that in fully external mixtures. The absorption coefficient of EC with internal mixture was, on average, 91% larger than that of fully external and EC/non-EC mixtures. It was also shown that the water content significantly influenced the aerosol optical properties during smog days as a result of high relative humidity and an increase in the water-soluble component.

This study developed an approach for estimating the optical properties of polydisperse aerosols. The calculated MEE depended strongly on the composition and assumed size distribution of aerosols. The computed MEE and MAE of EC had values of 0.728-13.481 $m^2\ g^{-1}$ and 0.3384-8.121 $m^2\ g^{-1}$, respectively, with the geometric mean diameters of 0.1-1 μm and geometric standard deviations of 1.3-2.2, which showed the significant impacts of the assumed aerosol size distributions on the MAE of EC. Although many studies have measured mass concentration in the bulk phase, composition-based size distribution information is still required for accurate calculations of aerosol optical properties. For example, MEE, MSE, and MAE can have significantly different values for the same mass concentration due to the assumed size distributions.

The sampling period of this study was only one week. During the spring of 2012, there was only one Asian dust event. The sampled PM2.5 measurements used in this study cannot cover all particle sizes (e.g., missing particles in the coarse mode), and a comparison of the ground based measurement with columnar observations clearly shows different behaviors. The sun photometer data refers only to diurnal and cloud free conditions, which differs from the 24 hour sampled data. More data with longer measurement period are required for future extended analysis, which should include estimation of the optical properties of WSOC and WISOC as well. Although the importance of aerosol size distribution, composition, and mixture state in the calculations of optical properties of aerosols is well recognized, large uncertainty still exists in their measurements due to difficulties and deficiencies in such measurements. Further, large variations due to both natural and anthropogenic causes hinder the accurate quantification of the radiative impacts of aerosols. However, obtaining such knowledge (e.g., Kawamura et al., 2004; Simoneit et al., 2004; Song et al., 2005; Kim et al., 2007; Kobayashi et al., 2007; Fu et al., 2012) is important and necessary for better understanding of the regional impacts of aerosols (e.g., radiative forcing of aerosol, Nakajima et al., 2003; Kim et al., 2005; Park et al., 2005; Chung et al., 2010; Huang et al., 2014), especially in East Asia, where large anthropogenic sources exist.

Appendix

The chemical composition based calculations of aerosol bulk optical properties proposed in this study require complex

calculations and assumptions of size distributions and mixture types of aerosols. The details of the developed model are described in this section.

a. Water contents

Water uptake by atmospheric particles affects their size and optical and chemical properties and, therefore, influences climate, deposition inside the humid respiratory tract, and corresponding health issues (Malm and Day, 2001; Engelhart et al., 2011). For calculations of aerosol optical properties, water contents as functions of aerosol composition and relative humidity can be obtained using a thermodynamic equilibrium model. In this study, SCAPE II (Simulating Composition of Atmospheric Particles at Equilibrium II) was used to calculate the water contents for a given chemical composition and relative humidity (Kim et al., 1993; Meng et al., 1998). The simulated results of water contents using the SCAPE II can be used to calculate aerosol optical properties including their hygroscopicity. This is closely related to relative humidity, which implies that the contribution of hygroscopicity is important for high relative humidity sampling cases.

b. Aerosol mixture

In this study, we tested three different types of aerosol mixture (i.e., internal mixture, fully external mixture, and EC/non-EC mixture) and compared their corresponding optical properties. A fully external mixture assumes that all the particles exist independently. Such mixtures can have different size distributions representing different compositions, and their optical properties can be calculated separately. An internal mixture assumes that all compositions are mixed within a single particle. In this mixture, the composition ratio can be assumed constant in order to represent the polydispersity of aerosols. The last assumption is that aerosol particles exist as either EC or all other (non-EC) particles. For this assumption, the remaining particles are assumed to be internally mixed (Jung et al., 2015). The aerosol optical properties corresponding to these three different mixtures were computed in this study.

c. Optical properties with polydisperse aerosol size distributions

Atmospheric aerosols are distributed over a broad range of sizes, and different representations of aerosol size distributions may cause different total optical properties of aerosols. In this study, size distributions of the ambient polydispersed aerosols are represented using a lognormal distribution function:

$$n(d_p) = \frac{N}{\sqrt{2\pi} d_p \ln\sigma_g} \exp\left[-\frac{\ln^2(d_p/d_g)}{2\ln^2\sigma_g}\right] \quad \text{(A1)}$$

where d_p is the diameter of the particle, d_g is the geometric mean diameter, σ_g is the geometric standard deviation, and N is the total aerosol number concentration. Eq. A1 can be converted to mass (volume) size distribution (Seinfeld and Pandis, 1998). The optical properties of the aerosols can then be calculated using the Mie theory.

The overall extinction coefficient (b_{ext}) of aerosols can be expressed as follows (Seinfeld and Pandis, 1998; Jung and Kim, 2007):

$$b_{ext} = \int_0^{d_p^{\max}} \frac{\pi d_p^2}{4} Q_{ext}(d_p, \lambda, m) n(d_p) dd_p \quad \text{(A2)}$$

Here, $Q_{ext}(d_p, \lambda, m)$ is the single particle extinction efficiency for a particle with a certain diameter (d_p), light wavelength (λ), and refractive index (m). The $n(d_p)$ is the size distribution.

The total removed energy (i.e., extinction) of incident light by a particle is the sum of scattered and absorbed energy by a particle. Thus, the corresponding single particle extinction efficiency is given by (Seinfeld and Pandis, 1998):

$$Q_{ext}(d_p, \lambda, m) = Q_{sca}(d_p, \lambda, m) + Q_{abs}(d_p, \lambda, m) \quad \text{(A3)}$$

where $Q_{sca}(d_p, \lambda, m)$ and $Q_{abs}(d_p, \lambda, m)$ are the single particle scattering and absorption efficiency, respectively.

The mass extinction efficiency (MEE) of the mass concentration (M), which is defined as the ratio of the extinction coefficient (b_{ext}) to the aerosol mass concentration, can be defined as follows (Hand and Malm, 2007):

$$MEE(M) = \frac{b_{ext}}{M} \quad \text{(A4)}$$

Likewise, the mass absorption efficiency (MAE) and mass scattering efficiency (MSE) can be defined as:

$$MAE(M) = \frac{b_{abs}}{M} \text{ and } MSE(M) = \frac{b_{sca}}{M} \quad \text{(A5)}$$

where b_{abs} and b_{sca} are the overall absorption and scattering coefficient, respectively. Combining Eqns. A2 and A3, the overall absorption and scattering coefficient can be expressed as:

$$b_{sca} = \int_0^{d_p^{\max}} \frac{\pi d_p^2}{4} Q_{sca}(d_p, \lambda, m) n(d_p) dd_p \text{ and}$$
$$b_{abs} = \int_0^{d_p^{\max}} \frac{\pi d_p^2}{4} Q_{abs}(d_p, \lambda, m) n(d_p) dd_p \quad \text{(A6)}$$

Acknowledgements. This research was supported by the Basic Science Research Program through the National Research Foundation of Korea (NRF), funded by the Ministry of Education (No. NRF-2015R1D1A1A09059906), and by the Korea Meteorological Administration Research and Development Program under Grant CATER 2014-3190. The authors gratefully acknowledge the NOAA Air Resources Laboratory (ARL) for the provision of the HYSPLIT transport and dispersion model and/or READY website (http://www.ready.noaa.gov) used in this research.

Edited by: Soon-Il An

References

Birch, M. E., and R. A. Cary, 1996: Elemental carbon-based method for monitoring occupational exposures to particulate diesel exhaust. *Aerosol Sci. Technol.*, **25**, 221-241.

Boreddy, S. K. R., and K. Kawamura, 2015: A 12-year observation of water-soluble ions in TSP aerosols collected at a remote marine location in the western North Pacific: An outflow region of Asian dust. *Atmos. Chem. Phys.*, **15**, 6437-6453, doi:10.5194/acp-15-6437-2015.

Chung, C. E., V. Ramanathan, G. Carmichael, S. Kulkarni, Y. Tang, B. Adhikary, L. R. Leung, and Y. Qian, 2010: Anthropogenic aerosol radiative forcing in Asia derived from regional models with atmospheric and aerosol data assimilation. *Atmos. Chem. Phys.,* **10**, 6007-6024, doi:10.5194/acp-10-6007-2010.

_____, K. Lee, and D. Müller, 2012: Effect of internal mixture on black carbon radiative forcing. *Tellus*, **64**, 10925, doi:10.3402/tellusb. v64i0. 10925.

Chylek, P., and J. A. Coakley, 1974: Aerosols and climate. *Science*, **183**, 75-77.

_____, and J. Wong, 1995: Effect of absorbing aerosols on global radiation budget. *Geophys. Res. Lett*, **22**, 929-931.

Draxler, R. R., and G. D. Hess, 1998: An overview of the HYSPLIT_4 modeling system for trajectories, dispersion, and deposition. *Australian Meteor. Mag.*, **47**, 295-308.

Engelhart, G. J., L. Hildebrandt, E. Kostenidou, N. Mihalopoulos, N. M. Donahue, and S. N. Pandis, 2011: Water content of aged aerosol. *Atmos. Chem. Phys.*, **11**, 911-920, doi:10.5194/acp-11-911-2011.

Facchini, M. C., M. Mircea, S. Fuzzi, and R. J. Charlson, 1999: Cloud albedo enhancement by surface-active organic solutes in growing droplets. *Nature*, **401**, 257-259.

Fu, H., M. Zhang, W. Li, J. Chen, L. Wang, X. Quan, and W. Wang, 2012: Morphology, composition and mixing state of individual carbonaceous aerosol in urban Shanghai. *Atmos. Chem. Phys.*, **12**, 693-707, doi:10. 5194/acp-12-693-2012.

Hand, J. L., and W. C. Malm, 2007: Review of aerosol mass scattering efficiencies from ground-based measurements since 1990. *J. Geophys. Res.*, **112**, D16203, doi:10.1029/2007JD008484.

Hess, M., P. Koepke, and I. Schult, 1998: Optical properties of aerosols and clouds: The software package OPAC. *Bull. Amer. Meteor. Soc.*, **79**, 831-844.

Horvath, H., M. Kasaharat, and P. Pesava, 1996: The size distribution and composition of the atmospheric aerosol at a rural and nearby urban location. *J. Aerosol Sci.*, **27**, 417-435.

Huang, K., G. Zhuang, Q. Wang, J. S. Fu, Y. Lin, T. Liu, L. Han, and C. Deng, 2014: Extreme haze pollution in Beijing during January 2013: Chemical characteristics, formation mechanism and role of fog processing. *Atmos. Chem. Phys. Discuss.*, **14**, 7517-7556, doi:10.5194/ acpd-14-7517-2014.

John, W., S. M. Wall, J. L. Ondo, and W. Winklmayr, 1990: Modes in the size distribution of atmospheric inorganic aerosols. *Atmos. Environ.*, **24**, 2349-2359.

Jung, C. H., and Y. P. Kim, 2007: Particle extinction coefficient for polydispersed aerosol using a harmonic mean type general approximated solution. *Aerosol Sci. Technol.*, **41**, 994-1001.

_____, J. Y. Lee, and Y. P. Kim, 2015: Estimation of aerosol optical properties considering hygroscopicity and light absorption. *Atmos. Environ.*, **105**, 191-201, doi:10.1016/j.atmosenv.2015.01.058.

Kawamura, K., M. Kobayashi, N. Tsubonuma, M. Mochida, T. Watanabe, and M. Lee, 2004: Organic and inorganic compositions of marine aerosols from east Asia: Seasonal variations of water-soluble dicarboxylic acids, major ions, total carbon and nitrogen, and stable C and N isotopic composition. *Geochem. Soc. Spec. Publ.*, **9**, 243-265.

Kim, D.-H., B. J. Sohn, T. Nakajima, and T. Takamura, 2005: Aerosol radiative forcing over east Asia from ground-based solar radiation measurements. *J. Geophys. Res.*, **110**, doi:10.1029/2004JD004678.

Kim, J., C. H. Jung, B.-C. Choi, S.-N. Oh, F. J. Brechtel, S.-C. Yoon, and S.-W. Kim, 2007: Number size distribution of atmospheric aerosols during ACE-Asia dust and precipitation events. *Atmos. Environ.*, **41**, 4841-4855.

Kim, Y. P., J. H. Seinfeld, and P. Saxena, 1993: Atmospheric gas-aerosol equilibrium I. Thermodynamic model. *Aerosol Sci. Technol.*, **19**, 157-181.

Kobayashi, H., K. Arao, T. Murayama, K. Iokibe, R. Koga, and M. Shiobara, 2007: High-resolution measurement of size distributions of Asian dust using a counter multisizer. *J. Atmos. Oceanic Technol.*, **24**, 194-205.

Lesins, G., P. Chylek, and U. Lohmann, 2002: A study of internal and external mixing scenarios and its effect on aerosol optical properties and direct radiative forcing. *J. Geophys. Res.*, **107**, 4094, doi:10.1029/ 2001JD000973.

Liu, C., C. E. Chung, F. Zhang, and Y. Yin, 2016: The colors of biomass burning aerosols in the atmosphere. *Sci. Rep.*, **6**, 28267, doi:10.1038/ srep28267.

Lohmann, U., and G. Lesins, 2002: Stronger constrains on the anthropogenic indirect aerosol effect. *Science*, **298**, 1012-1015.

_____, and J. Feichter, 2005: Global indirect aerosol effects: A review. *Atmos. Chem. Phys.*, **5**, 715-737.

Malm, W. C., and D. E. Day, 2001: Estimates of aerosol species scattering characteristics as a function of relative humidity. *Atmos. Environ.*, **35**, 2845-2860, doi:10.1016/S1352-2310(01)00077-2.

Meng, Z., D. Dabdub, and J. H. Seinfeld, 1998: Size-resolved and chemically resolved model of atmospheric aerosol dynamics. *J. Geophys. Res.*, **103**, 3419-3435.

Nakajima, T., and Coauthors, 2003: Significance of direct and indirect radiative forcings of aerosols in the East China Sea region. *J. Geophys. Res.*, **108**, doi:10.1029/2002JD003261.

Park, S.-U., L.-S. Chang, and E.-H. Lee, 2005: Direct radiative forcing due to aerosols in East Asia during a Hwangsa (Asian dust) event observed on 19-23 March 2002 in Korea. *Atmos. Environ.*, **39**, 2593-2606.

Saxena, P., and L. M. Hildemann, 1996: Water-soluble organics in atmospheric particles: A critical review of the literature and application of thermodynamics to identify candidate compounds. *J. Atmos. Chem.*, **24**, 57-109.

Schulz, M., and Coauthors, 2006: Radiative forcing by aerosols as derived from the AeroCom present-day and pre-industrial simulations, *Atmos. Chem. Phys.*, **6**, 5225-5246.

Seinfeld, J. H., and S. N. Pandis, 1998: Atmospheric Chemistry and Physics: From Air Pollution to Climate Change. John Wiley, 1326 pp.

Simoneit, B. R. T., M. Kobayashi, M. Mochida, K. Kawamura, M. Lee, H.-J. Lim, B. J. Turpin, and Y. Komazaki, 2004: Composition and major sources of organic compounds of aerosol particulate matter sampled during the ACE-Asia campaign. *J. Geophys. Res.*, **109**, D19S10, doi:10.1029/2004JD004598.

Song, C. H., Y. Ma, D. Orsini, Y. P. Kim, and R. J. Weber, 2005: An investigation into the ionic chemical composition and mixing state of biomass burning particles recorded during TRACE-P P3B Flight#10. *J. Atmos. Chem.*, **51**, 43-64.

Textor, C., and Coauthors, 2006: Analysis and quantification of the diversities of aerosol life cycles within AeroCom. *Atmos. Chem. Phys.*, **6**, 1777-1813.

Turpin, B. J., and H.-J. Lim, 2001: Species contributions to PM2.5 mass concentrations: Revisiting common assumptions for estimating organic mass. *Aerosol Sci. Technol.*, **35**, 602-610.